The effect of illumination on *p-n* junction diodes based on Yb-doped CuO thin films produced by ultrasonic spray pyrolysis method

Havva Elif Lapa[1],* ⓘ

[1] *Department of Energy Systems Engineering, Graduate Education Institute, Isparta University of Applied Sciences, 32260 Isparta, Turkey*

ABSTRACT

On the glass substrate, un-doped and different proportions of Yb (1, 2, 3, 4, and 5 wt%) doped CuO thin films were deposited by the ultrasonic spray pyrolysis (USP) method. According to X-ray diffraction (XRD) analysis, the (− 111) plane was the preferred crystallographic orientation for all thin films. It was obtained from atomic force microscopy (AFM) analysis that the surfaces of the produced CuO thin films were not smooth and the roughness increased as the Yb doping ratio increased. Scanning electron microscopy (SEM) analysis reveals that the surfaces of 4 and 5 wt% Yb-doped CuO thin films were porous. The forbidden bandgap values of un-doped and 1, 2, 3, 4, and 5 wt% Yb-doped CuO thin films were calculated by using the Tauc plot. It was observed that 3 wt% Yb-doped CuO thin films with the narrowest bandgap of 1.64 eV. The 3 wt% Yb-doped CuO thin films were deposited on both non-etched and KOH-etched *n*-type Si by the USP method, and so, *p*-CuO/*n*-Si *p-n* junction diodes were produced. The influence of illumination on several electrical properties of the generated *p-n* diodes, such as ideality factor (n), zero-bias barrier height (Φ_{bo}), and series resistance (R_s), was examined. The *p*-CuO (un-doped and 3 wt% doped Yb)/*n*-Si (KOH-etched) diodes exhibited photovoltaic behavior. These diodes show promise for photodiode applications in the optoelectronics industry.

1 Introduction

In order to develop innovative technologies, researchers are focusing on energy storage and conversion devices that are light, eco-friendly, and low-cost. Metal oxide semiconductor nanostructured energy materials used as components of devices, such as *p-n* junction transistors, solar cells, fuel cells, gas sensors, and capacitors are notable in the electronics and optoelectronics industries [1–5]. Among these metal oxides, cupric oxide, or copper (II) oxide (CuO), is abundant on earth, non-toxic, and easily synthesized. The monoclinic CuO phase is thought to be the most stable of the Cu–O compound's crystal

Address correspondence to E-mail: h.eliflapa@gmail.com

structures. CuO thin films are p-type semiconductors and their bandgaps are in the range of 1.3–2.1 eV [6, 7].

The CuO thin films were produced with different methods such as chemical bath deposition, spin coating, plasma evaporation, spray pyrolysis, and ultrasonic spray pyrolysis (USP) [8–12]. The USP technique is solution-based and allows selection of solvent for product morphology. The pyrolysis temperature and nozzle frequency can be adjusted in this production method. Thus, the USP is a more flexible production technique compared to other methods. It is also an ideal method for producing thin films with both a wide area and the desired surface morphology. Thin films with small-grained, porous, and compact structures, which are very effective in solar cell and sensor applications, can be obtained by using this method [13]. The USP method is an economical method as it saves material [14]. The quality of the thin film deposited on the substrate is affected by the distance of the nozzle from the substrate, nozzle diameter, solution flow rate, and substrate temperature [15, 16]. These parameters can be easily controlled by the USP method.

CuO thin films are used as components of devices such as p-n junction diodes, solar cells, and supercapacitors [11, 17, 18]. These thin films are preferred as absorber layers in solar cells due to their chemical and electrical properties. Low conductivity and high electron-hole recombination can limit the performance of a device. Therefore, the efficiency of the device can be improved by making appropriate doping of CuO. According to Ahmed et al. the 2% Ba-doped CuO films demonstrate good photocatalytic activity as a photoelectrode for efficient hydrogen production [7]. Yin et al. showed that Ni doping modulates the crystal quality, shape, and grain size of $Cu_{1-x}Ni_xO$ thin films [19]. Ytterbium (Yb) is a rare-earth metal, and it is a member of the lanthanide series in the periodic table. It exhibits two different oxidation states of + 2 and + 3. It is known to be used as a dopant in optical materials. Yb^{+3} has a larger ionic radius (0.86 Å) than Cu^{+2} (0.73 Å) [20, 21]. The electronegativity value for Yb^{+3} is 1.1 Pauling, while this value is 1.9 Pauling for Cu^{+2} [22]. It is clear that the Yb doping to the CuO lattice will have an effect on the electrical, optical, and structural morphology of CuO thin films. Naveena et al. prepared un-doped and Yb-doped CuO thin films by chemical spray pyrolysis [11]. When compared to un-doped CuO thin films, they found that the doped CuO thin films with Yb (3 wt%) had better carrier concentration, electrical conductivity, and power conversion efficiency.

In this work, the un-doped and different proportions of Yb (1, 2, 3, 4, and 5 wt%) doped CuO thin films were deposited on soda-lime glass substrates by the USP method. X-ray diffraction (XRD), scanning electron microscopy (SEM), atomic force microscopy (AFM), and ultraviolet-visible (UV/Vis) spectrophotometer were used to evaluate the effect of Yb doping on the structural, morphological, and optical properties of CuO thin films. The p-CuO (3 wt% Yb-doped)/n-Si p-n junction diodes were fabricated by the USP method on both non-etched and KOH-etched n-Si. The current-voltage (I-V) characteristics of the diodes were used to determine their electrical properties. The effects of illumination on I−V characteristics were investigated. There is no known study in the literature on the deposition of Yb-doped CuO thin films on KOH-etched Si surfaces by the USP method. The effect of illumination on Ag/p-CuO (3 wt% Yb-doped)/n-Si (KOH-etched)/Al junction diodes was also noted to have not been studied.

2 Experimental

The un-doped and Yb-doped CuO thin films were deposited on soda-lime glass substrates of 2.5 cm × 2.5 cm × 0.2 mm dimension by using the USP method. The substrates were ultrasonically cleaned with double distilled water, ethanol, acetone, and ethanol at 60 °C for 10 min. The cleaned glass substrates were rinsed with double distilled water and dried with N_2 gas. Copper (II) acetate monohydrate ($Cu(CH_3COO)_2 \cdot H_2O$) was the precursor material for the copper source. A solution of 0.1 M $Cu(CH_3COO)_2 \cdot H_2O$ was prepared. Double distilled water was used as the solvent. 0.1 mL of HCl (37%) was added to the prepared solution. Thus, better adhesion of the material to the substrate surface is achieved. The ytterbium chloride hexahydrate ($YbCl_3 \cdot 6H_2O$) was used for Yb doping, and it was doped different proportions of 1, 2, 3, 4, and 5 wt%. The solutions were stirred for 45 min at room temperature using a magnetic stirrer. A homogeneous solution was obtained. The parameters used in the USP device (Sono-Tek Corporation, 2012 Route 9 W) for the production of CuO thin films are given in

Table 1. Schematic representations of the solution preparation and the USP coating system are given in Fig. 1a and b, respectively. Thin films were annealed at 525 °C for 1 h in the muffle furnace. The hot probe method was used to determine whether the created films were p-type.

XRD measurements of the thin films were taken in the range of 20–80° using the Cu Kα radiation (λ = 1.5418 Å) of a Bruker D8 Advance Twin–Twin diffractometer (40 kV, 40 mA). Raman measurements were performed with a JASCO NRS-3100 spectrophotometer equipped with a laser diode emitting at 785 nm. The surface morphologies of the films were observed by SEM (FEI Quanta FEG 250), while the surface roughness was examined by AFM (Nanomagnetics ezAFM). Optical absorption studies of thin films were carried out with a UV-Vis Spectrophotometer (PG-Instruments T80+) operated at room temperature.

The Ag/p-CuO (un-doped and 3 wt% Yb-doped)/n-Si/Al p-n junction diodes were manufactured. [100] oriented n-type Si wafers were used. A wet chemical process was used to clean the n-Si wafers of organic and inorganic impurities [23]. These wafers were dipped in a potassium hydroxide (KOH) solution (1 g KOH:5 mL 2-propanol (IPA): 125 mL double distilled water) at 80 °C for 10 min to etch their surface. The wafers were cleaned with acetone and ethanol, and then rinsed with double distilled water. The cleaned wafers were exposed to hydrofluoric acid (HF) for 3 min and then dried with N_2 gas.

By the thermal evaporation method, Al was evaporated to the back surface of both non-etched and KOH-etched n-Si wafers. Then, these wafers were annealed at 575 °C in an N_2 ambiance for 3 min. Thus, the ohmic contact process is completed. The un-doped and 3 wt% Yb-doped CuO thin films were

Table 1 Parameters used for the production of CuO thin films

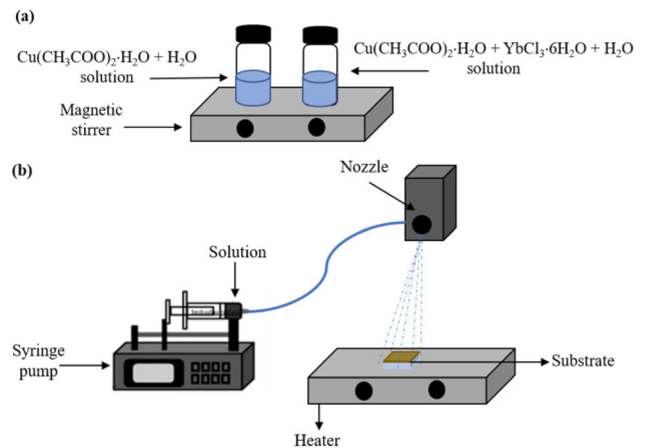| Parameters	Values
Substrate temperature (°C)	350
Solution flow rate (mL/min)	0.2
Distance of the nozzle to the substrate (cm)	8.5
Nozzle gas pressure (kPa)	1.0
Nozzle diameter (mm)	0.2
Spray angle (°)	90
Spray frequency (kHz)	120
Spray engine power (W)	5.33

**Fig. 1** Schematic representations of **a** the solution preparation **b** the USP coating system

deposited on the front surfaces of both etched and non-etched n-Si wafers by the USP method, and then annealed at 525 °C for 1 h. The annealing process is needed for two reasons. The first is to perform the thermal decomposition of copper (II) acetate monohydrate and to form CuO. The second is to ensure the formation of a good crystal structure for CuO [24, 25]. The coating parameters given in Table 1 were used. The mask, which have square area of 4 mm^2, was placed on the front surface of the annealed structures, and Ag was thermally evaporated. Thus, the manufacture of Ag/p-CuO/n-Si/Al, Ag/p-CuO (Yb-doped)/n-Si/Al, Ag/p-CuO/n-Si (KOH-etched)/Al, and Ag/p-CuO (Yb-doped)/n-Si (KOH-etched)/Al p-n junction diodes was completed and were named as S1, S2, S3, and S4, respectively. The schematic representation of the produced p-n junctions is given in Fig. 2.

I-V measurements of the produced p-n junctions were taken in the dark and under illumination (1040 Wm^{-2}) with the Keithley 2400 SourceMeter at ± 2 V range at room temperature. The p-n junctions were illuminated by using a solar simulator (Model: Solar Light). The density of illumination was controlled with a research radiometer (Model ILT1700). The solar spectrum was simulated with an AM 1.5 filter.

3 Results and discussed

The XRD patterns of un-doped and Yb-doped CuO films grown on glass substrates using the USP method are shown in Fig. 3. Thin films have two peaks in the (−111) and (111) planes. According to

Fig. 2 The schematic representation of the produced p-n junctions
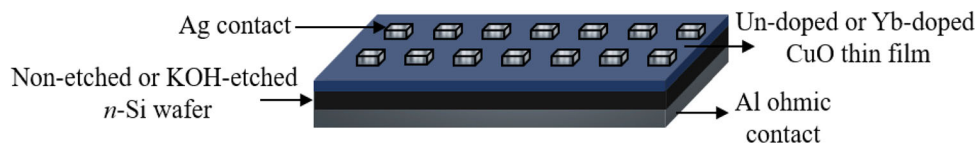
the ICDD PDF-00-001-1117 card, these diffraction peaks belong to the monoclinic CuO. These peaks were observed at 35.74° and 38.95° for un-doped CuO. The (−111) plane has a higher density peak for all thin films. This indicates that the (−111) plane is the preferred crystalline plane. The formation of the crystallite in the deposited thin films means that sufficient thermal energy is provided for the pyrolysis of the precursor material. No phase formation related to Yb (Yb_2O_3, YbO) was detected. No Cu_2O phase or any other impurity phase was found. Such a situation confirms that chemically pure, Yb-doped, and single-phase CuO were formed. A small shift in peak positions was observed when Yb-doped CuO was compared to un-doped CuO (inset of Fig. 3). This is due to Yb^{+3} having a higher ionic radius (0.86 Å) than Cu^{+2} (0.73 Å) [11].

The average crystallite size (D) of un-doped and Yb-doped thin films can be calculated using the Debye-Scherrer equation, which is given by the following equation [26]:

$$D = \frac{0.94\lambda}{\beta \cos\theta}. \tag{1}$$

Here, θ is the diffraction angle of the maximum intensity peak, β is the half peak width (in radians) of the maximum intensity peak, and λ is the x-ray wavelength. XRD measurements were taken with Bruker's D8 Advance Twin-Twin device, and analyses were carried out by the same company's EVA software and ICDD database. The (−111) peak is sharp, and its intensity is higher than that of the other peak. Therefore, this peak was chosen as the main peak. Crystallite sizes were calculated from the FWHM (full width at half maximum) values of the main peak. These calculations were made in software by the EVA program using the Debye-Scherrer equation. The values obtained for the crystallite sizes are given in Table 2.

The crystallite size for un-doped CuO thin films was obtained as 200 Å whereas this value was decreased for 1, 2 and 3 wt% Yb doping to CuO thin films. The values of crystallite size of 4 and 5 wt% Yb-doped CuO thin films are higher than other thin films crystallite sizes. Similar results were observed for Ba-doped CuO and this case was attributed to shift in the peaks due to doping and the change in the FWHM value [7].

The Raman spectra of un-doped and Yb-doped CuO thin films are given in Fig. 4. Measurements were registered in the wavelength interval of 200–700 cm^{-1} and at room temperature. In the primitive cell, two molecular units of monoclinic CuO are formed. There are 12 modes of zone-
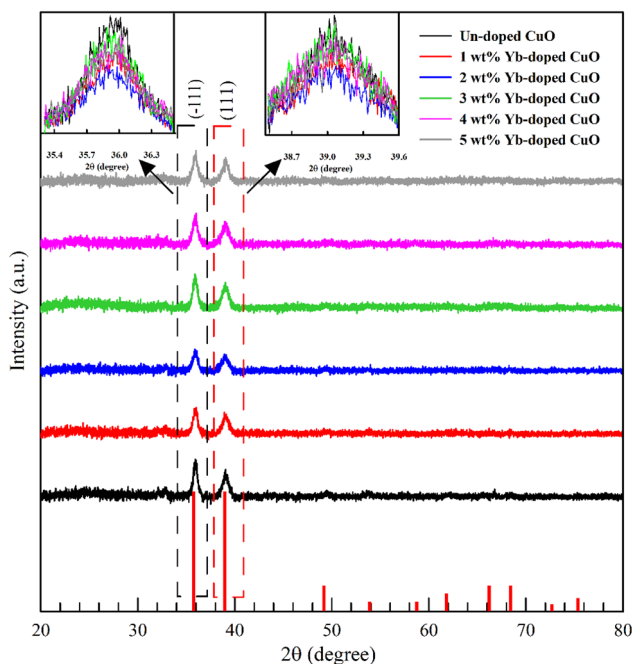

Fig. 3 XRD patterns of un-doped CuO and Yb-doped CuO thin films. Position change due to Yb doping in the (−111) plane (inset)

Table 2 The size of crystallites in un-doped and Yb-doped CuO thin films

Sample	Crystallite size (Å)
Un-doped	200
1 wt% Yb-doped	184
2 wt% Yb-doped	174
3 wt% Yb-doped	181
4 wt% Yb-doped	215
5 wt% Yb-doped	229

centered optical phonons, $4A_u + 5B_u + A_g + 2B_g$, three of which $A_g + 2B_g$ are the Raman active modes [27, 28]. In this study, three main phonon modes at 310, 371 and 612 cm^{-1} were observed from Raman spectrum of the un-doped CuO thin films. These modes are corresponding to A_g, B_{1g} and B_{2g} symmetries, respectively. Similar peaks have been reported in the literature for CuO (Table 3). Similar peaks in the Raman spectra were also observed for Yb-doped CuO thin films. The peaks in the Yb-doped CuO thin film spectra almost matched the un-doped CuO thin films. Extra peaks are not observed for the Yb-doped CuO thin films. Therefore, it can be concluded that there is no new phase appearance due to Yb doping. This result is compatible with the XRD results.

AFM was used to examine the surface morphologies of un-doped and Yb-doped CuO thin films. The AFM images of un-doped and 1, 2, 3, 4, and 5 wt% Yb-doped CuO thin films are shown in Fig. 5a–f, respectively.

The surface roughness of un-doped and 1, 2, 3, 4, and 5 wt% Yb-doped CuO thin films was found to be 33.31, 52.63, 58.27, 59.03, 66.31, and 72.97 nm, respectively. The surfaces of the produced films are not smooth, and the roughness increases as the Yb-doped ratio increases. The use of rough interfaces in solar cells causes an increase in light absorption. The
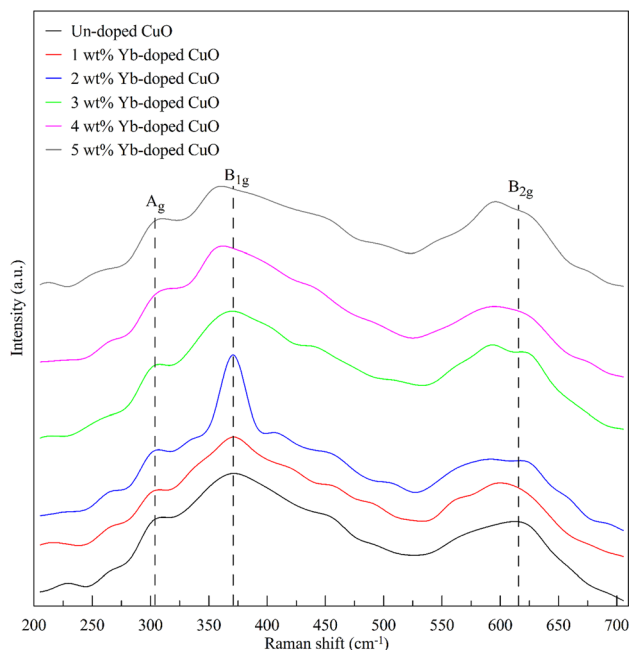
use of chemically active area layers in gas sensors increases the rate at which gas diffuses from the pores. Therefore, rough surface morphology is important in device applications based on metal oxide thin films.

SEM images (surface and cross-sectional) of un-doped and 1, 2, 3, 4, and 5 wt% Yb-doped CuO thin films are given in Fig. 6a–f, respectively. As can be seen from Fig. 6a–f, the CuO thin films were generated by a random dispersion of shaped nanoparticles. According to SEM images, the glass substrate surface is completely covered with CuO, and all of the CuO thin films have an irregular particle size and rough surface. The crystallite sizes of CuO thin films were calculated using the Debye-Scherrer equation, while the particle sizes were determined using SEM-surface images. Particle sizes were shown on the SEM-surface images for un-doped and 5 wt% Yb-doped CuO thin films (were given in Fig. 6a and f). While the average particle size was calculated as 37.48 nm for un-doped CuO thin film, it was obtained as 80.82 nm for 5 wt% Yb-doped CuO thin film. For high Yb-doped ratios (4 and 5 wt%), aggregation occurred on the surface of the CuO thin films. It has been observed in the literature that particle sizes increase with the doping of elements such as Ba, Yb, and Er in CuO thin films [7, 11, 29]. In addition, it is seen that the surface of the 3 wt% Yb-doped CuO thin film is coated more homogeneously than all other surfaces. It was observed that the film surfaces of 4 wt% and 5 wt% Yb-doped CuO thin films were porous compared to the others. It is seen that the surface morphology and particle size of CuO thin films are affected by Yb doping. The thicknesses of the films are 180.8, 277.9, 294.1, 407.4, 313, and 348 nm for un-doped, 1, 2, 3, 4, and 5 wt% Yb-doped to CuO thin films, respectively (inset of Fig. 6a–f).

Optical transmittance measurements of un-doped and Yb-doped CuO thin films deposited on glass substrates were carried out in the wavelength range of 290–1100 nm. The wavelength dependent plots of the transmittance of the produced thin films are shown in Fig. 7a. The transmittance value for un-doped CuO thin films averages 12% in the visible regions (390–780 nm). The transmittance values for 1, 2, 3, 4, and 5 wt% Yb-doped CuO thin films are 19, 15, 10, 14, and 11% at the same region, respectively.

The following equation can be used to express the relationship between optical bandgap and absorption coefficient [30]:
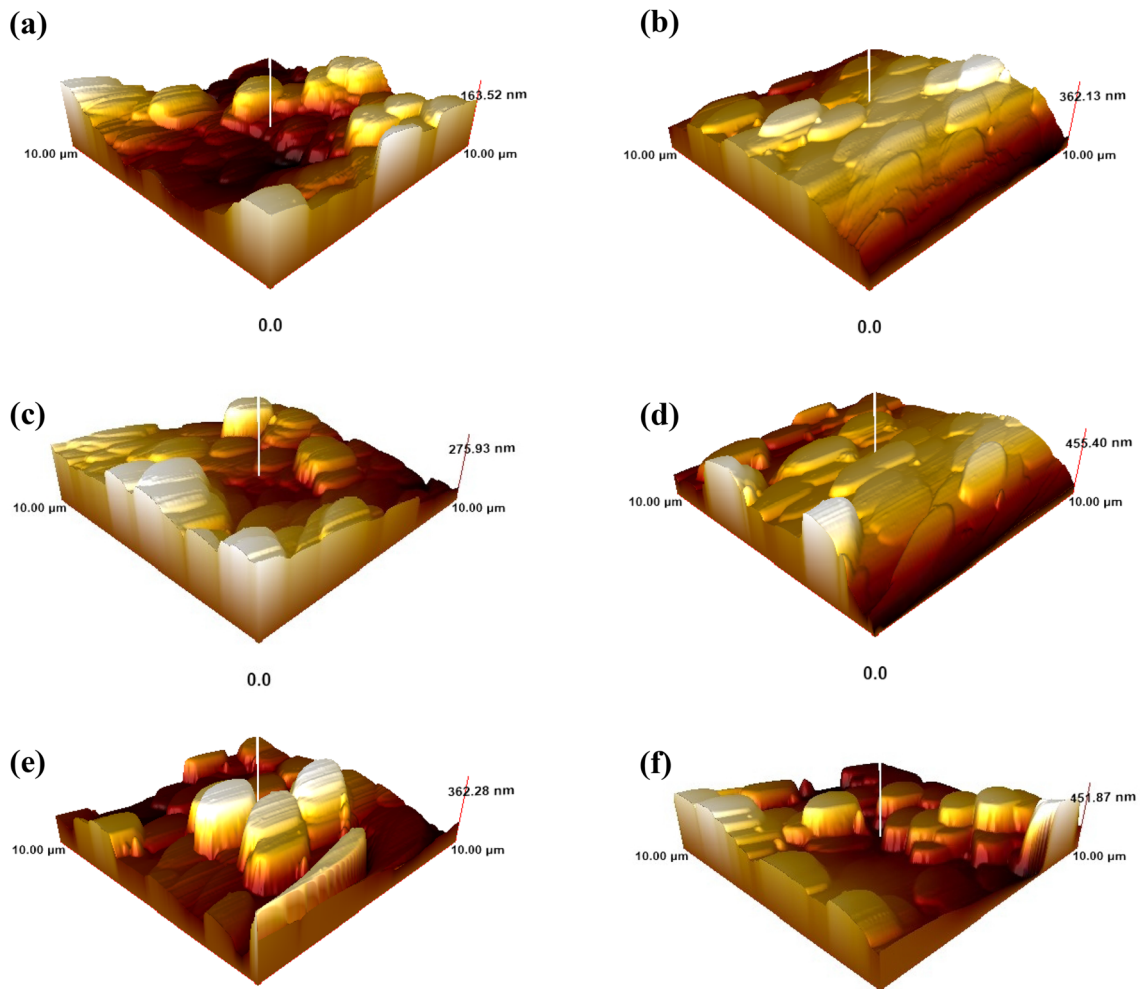

Fig. 4 Raman spectra of un-doped CuO and Yb-doped CuO thin films

Fig. 5 AFMimages of the **a** un-doped **b** 1 wt% **c** 2 wt% **d** 3 wt% **e** 4 wt% **f** 5 wt% Yb-doped CuOthin films

$$\alpha h v = A(h v - E_g)^n. \tag{2}$$

In this expression, α is the absorption coefficient, h is the Planck's constant, v is the frequency of the incident photon, A is an energy independent constant, and E_g is the forbidden bandgap of the semiconductor. In semiconductors with a direct bandgap, n is equal to $1/2$. The Tauc curve is obtained by plotting $(\alpha h v)^2$ according to $h v$ and the E_g value can be found from the point where this curve cuts the x-axis. Tauc plots of un-doped and different proportions of Yb-doped CuO thin films are shown in Fig. 7b. The E_g values for un-doped and 1, 2, 3, 4, and 5 wt% Yb-doped CuO thin films are 1.68, 1.77, 1.74, 1.64, 1.71, and 1.65 eV, respectively.

Optical reflections on the Si wafer surface can be controlled by etching the wafer surface with KOH. Pyramidal and non-pyramidal structures of different sizes can occur on the Si surface etched with KOH. Thus, textured surfaces can obtained. These textured surfaces may absorb more light than flat surfaces, thereby effectively reducing the reflection of light in the solar cell. This can lead to an increase in solar cell efficiency [31]. Cross-sectional SEM images of S1, S2, S3 and S4 *p-n* junction diodes are given in Fig. 8a–d (it can be taken at 50,000 × and 100,000 × magnifications), respectively.

Figure 8a and b shows no pyramidal structures. The un-doped CuO thin film was deposited almost homogeneously on the non-etch *n*-Si wafer by the USP method (Fig. 8a). Randomly dispersed particles may result from droplets of 3 wt% Yb-doped CuO falling to the non-etch *n*-Si wafer surface (Fig. 8b). In Fig. 8c and d 3 wt% Yb-doped CuO and Ag coated on pyramidal structures of different sizes are observed.

The reverse and forward bias *I-V* characteristics both in the dark and under illumination of prepared
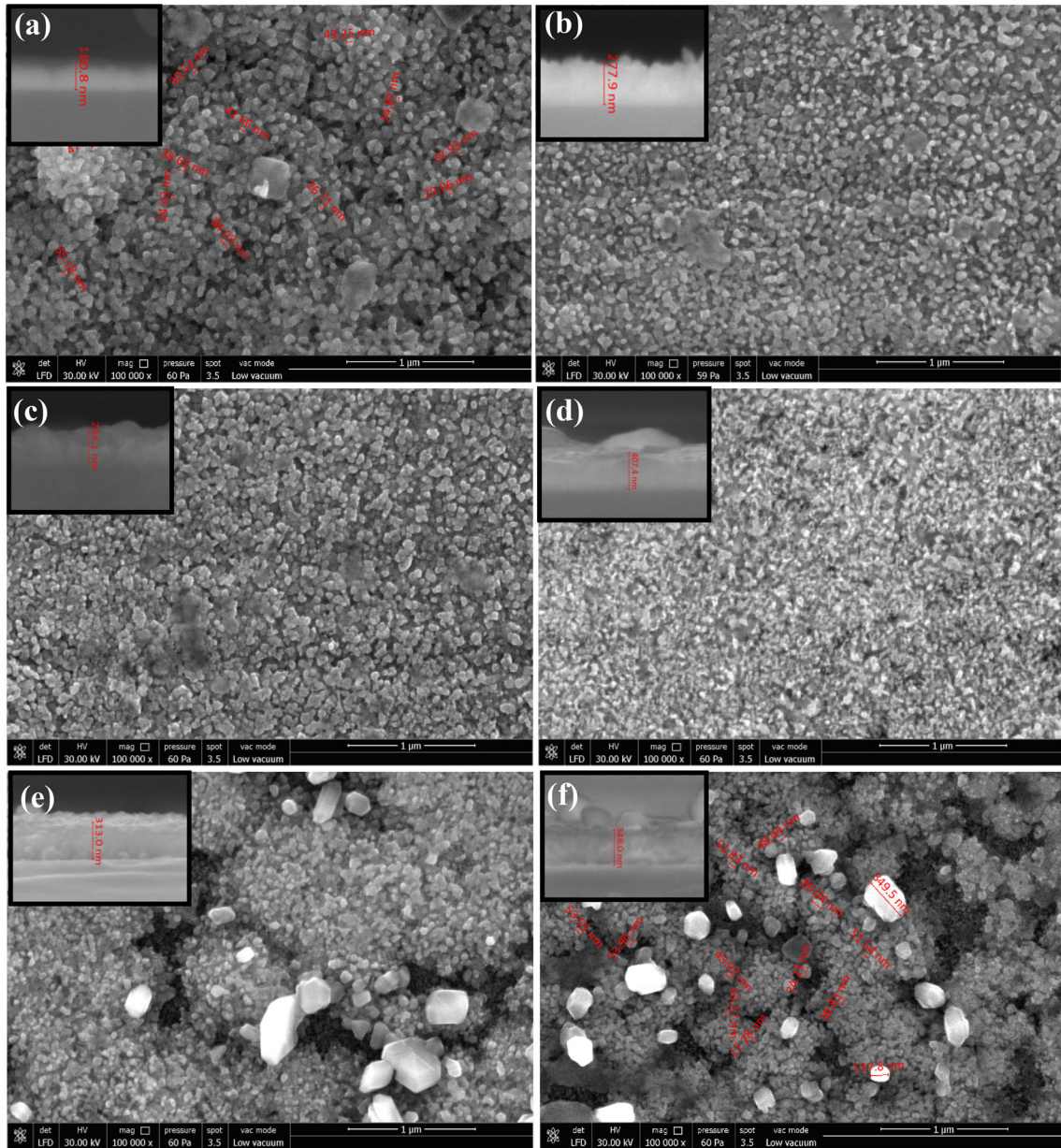
Fig. 6 SEM images of the **a** un-doped **b** 1 wt% **c** 2 wt% **d** 3 wt% **e** 4 wt% **f** 5 wt% Yb-doped CuO thin films. Film thicknesses for un-doped and Yb-doped CuO thin films (inset)

p-n junction diodes were presented in Fig. 9. *I-V* characteristics of S1 and S2 *p-n* junction diodes constructed by using non-etched *n*-Si wafer are given in Fig. 9a. *I-V* characteristics of S3 and S4 *p-n* junction diodes constructed by using KOH-etched *n*-Si wafer are given in Fig. 9b. The forward bias *I-V* curves for each diode have a linear region and the current values increase with illumination. These curves bend after a certain forward applied voltage. This bending may be caused by the series resistance (R_s) effect [32].

The R_s value can be simply calculated by using Ohm's law ($R_s = dV/dI$). R_s values were calculated for prepared diodes both in the dark and under illumination and are given in Table 4.

The S1 diodes exhibit photodiode properties under illumination (Fig. 9a). Similar *I-V* characteristics under illumination have been found for *p*-CuO/*n*-Si *p-n* junction diodes in the literature [17]. In the dark, S2 diodes have a good rectification ratio ($RR = I_{forward}/I_{reverse}$) compared to other diodes (Fig. 9a and b).
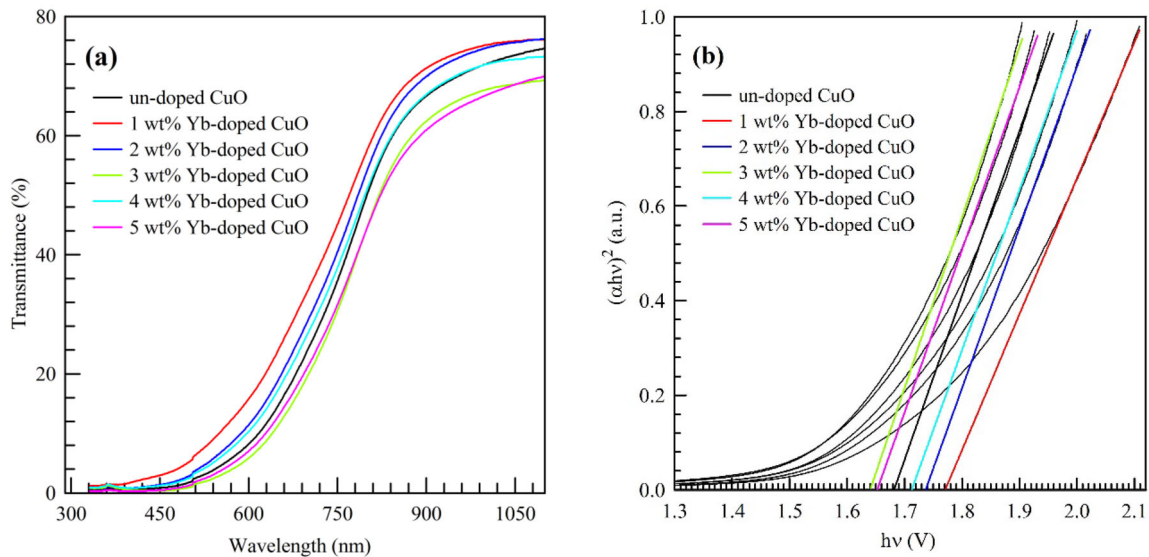
Fig. 7 For un-doped and 1, 2, 3, 4, and 5 wt% Yb-doped CuO thin films **a** the wavelength dependent plots of the transmittance **b** Tauc plots
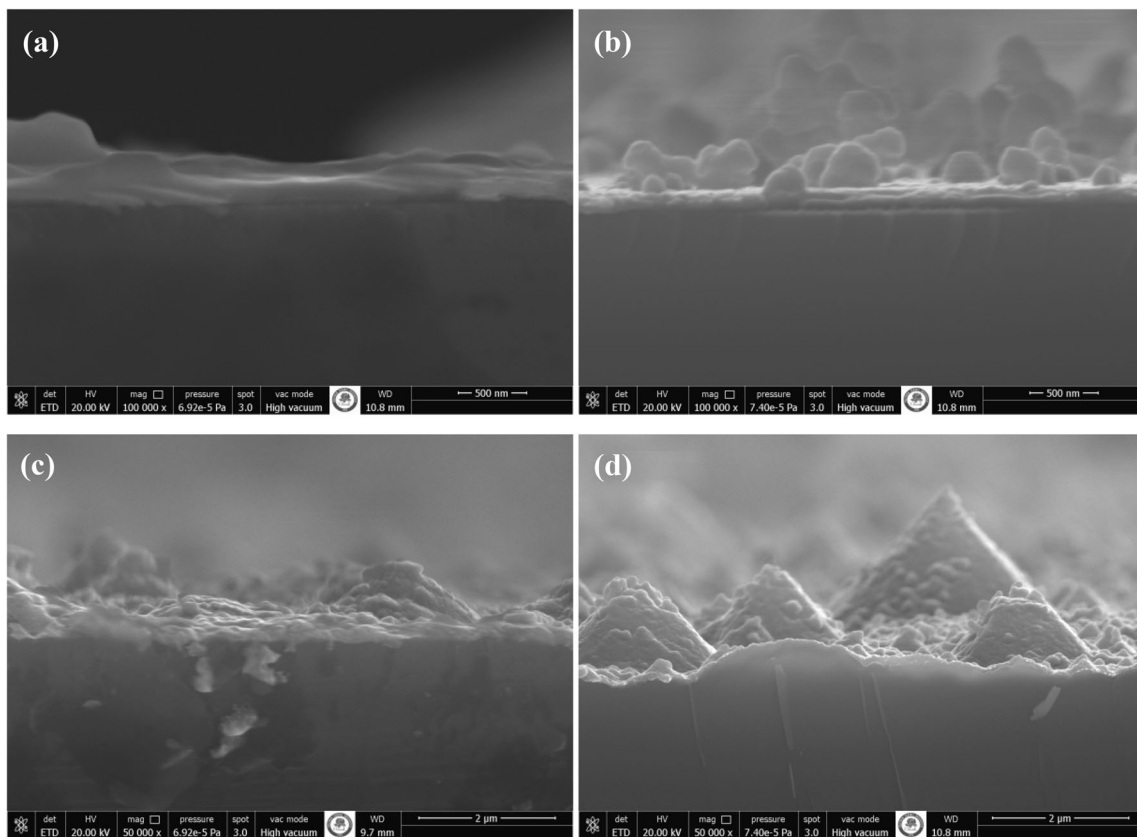

Fig. 8 The cross-sectional images of **a** S1 **b** S2 **c** S3 **d** S4 *p-n* junction diodes

The *RR* value for the S2 diode in the dark was calculated as 422.4.

Rectification is a common phenomenon in diodes used in circuits requiring fast switching speeds [32, 33]. Doping CuO thin films with 3 wt% Yb improved the *RR* property of Ag/*p*-CuO/(non-etched) *n*-Si *p-n* junction diodes. It is seen that the current-voltage curve of the S2 diode shifts to the left
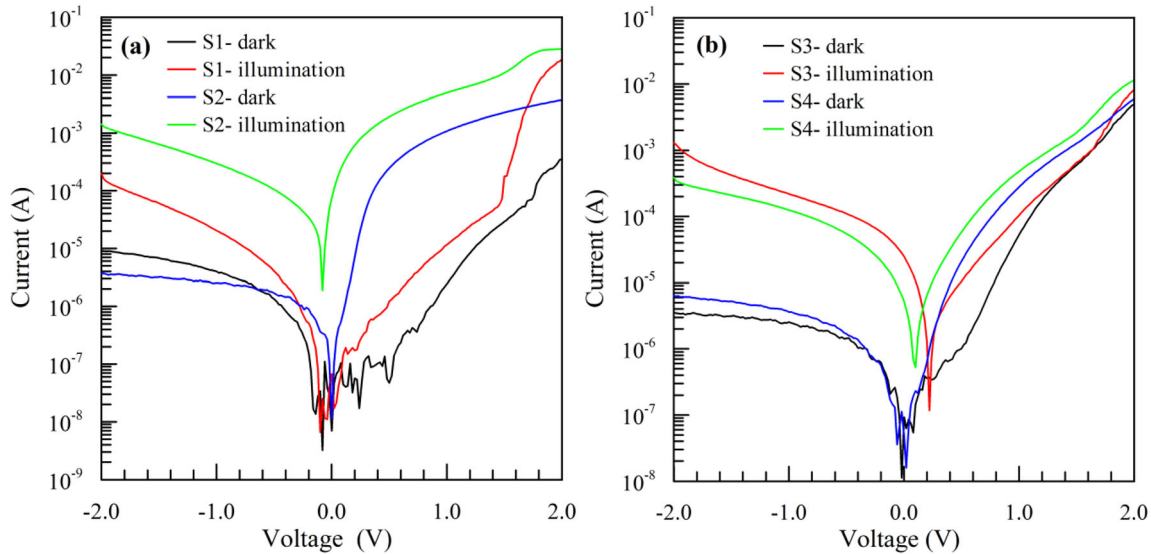
Fig. 9 I-V characteristics of S1, S2, S3, and S4 p-n junction diodes both in the dark and under illumination **a** deposited on n-Si wafer **b** deposited on KOH-etch n-Si wafer

Table 3 Parameters obtained from Raman spectroscopy

Symmetries	Activity	This work (cm^{-1})	Other works (cm^{-1})
A_g	Raman	310	319 [27, 28]
B_g	Raman	371	382 [27, 28]
B_g	Raman	612	631 [27, 28]

under illumination. The ferroelectric property of Ag/ p-CuO/(non-etched) n-Si p-n junction diodes may have been provided by Yb doping to CuO thin films. It is seen that the S3 and S4 diodes exhibit photovoltaic properties under illumination (Fig. 9b). This may be due to the fact that the pyramidal structures (Fig. 8c and d) formed on the Si surface etched with KOH reduce the reflection of incident light.

For p-n junction diodes, the relationship between I and V can be expressed as [34]:

$$I = I_o \left[\exp\left(\frac{qV}{nkT}\right) - 1 \right]. \tag{3}$$

Here, I_o is the saturation current, V is the applied voltage, k is the Boltzmann constant, T is the absolute temperature, and n is the ideality factor. According to the Shockley theory [34], n = 1 for p-n junctions in the absence of recombination. The component of the straight-line intercept of the semi-logarithmic I-V plot can be used to calculate the I_o value. The following formula can be used to calculate n and Φ_{bo} values [34]:

$$n = \frac{q}{kT} \frac{dV}{d(\ln(I))}, \tag{4}$$

$$\Phi_{bo} = \frac{kT}{q} \ln\left(\frac{AA^*T^2}{I_o}\right). \tag{5}$$

Here, A^* is the effective Richardson constant (= 112 Acm^{-2} K^{-2} for n-Si [34]). n and Φ_{bo} values were calculated for prepared diodes both in the dark and under illumination and are given in Table 4.

From Table 4, it can be seen that the electrical parameters of the diodes are affected by the doping of Yb to CuO and the KOH etch of Si wafer. The n values of all produced diodes are higher than the ideal value (n = 1). A high R_s value can cause a high ideality factor. The R_s limits the current flow in the circuit and this can cause the diode to deviate from the ideality [32, 34]. It is seen that n and R_s values decrease with Yb doping for diodes fabricated on both non-etched and KOH-etched Si wafer. The n values of all produced diodes increased under illumination whereas the Φ_{bo} and R_s values decreased.

In p-n junction diodes, photovoltaic parameters such as short-circuit current density (J_{sc}) and open-circuit voltage (V_{oc}) can be determined by using the fourth region of the current density-voltage (J-V) graph. The J-V curves drawn for the fourth region of the S3 and S4 diodes are given in Fig. 10.

V_{oc} and J_{sc} values were found from the points where the curve of J-V intersects the voltage and

Table 4 Some electrical parameters derived from the *I-V* characteristics of prepared *p-n* junction diodes

Sample	Dark			Illumination		
	n	Φ_{bo} (eV)	R_s (Ω)	n	Φ_{bo} (eV)	R_s (Ω)
S1	6.18	0.68	5697.2	8.25	0.60	107.3
S2	1.77	0.61	533.5	4.40	0.42	70.4
S3	4.50	0.66	399	8.43	0.54	243.4
S4	2.60	0.63	335.1	3.02	0.56	174.4
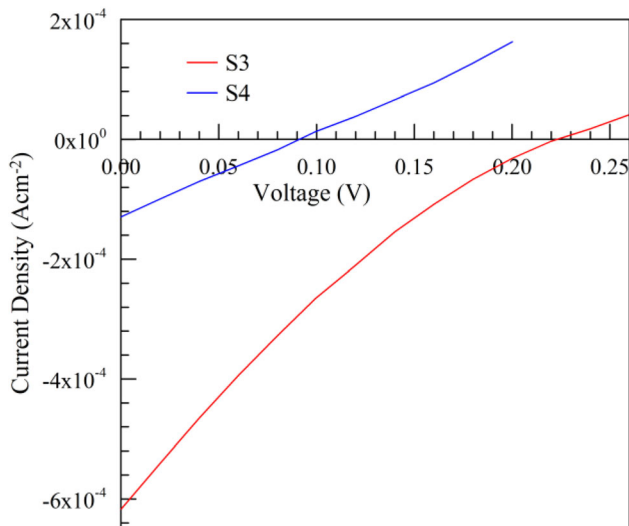
Fig. 10 The fourth quarter of the *J-V* characteristics of the S3 and S4 *p-n* junction diodes under illumination

current density axis in this region, respectively. V_{oc} values for the S3 and S4 diodes were obtained as 0.22 and 0.09 V, respectively. J_{sc} values for the S3 and S4 diodes were obtained as 6.17×10^{-4} Acm^{-2} and 1.30×10^{-4} Acm^{-2}, respectively. A higher V_{oc} value was obtained for *p*-CuO/*n*-Si *p-n* junction diodes produced by using KOH-etched *n*-Si wafer and un-doped CuO thin films. The J_m and V_m values are determined by the fourth region of the *J-V* characteristic [35]. V_m values for the S3 and S4 diodes were obtained as 0.10 V and 0.04 V, respectively. J_m values for the S3 and S4 diodes were obtained as 2.65×10^{-4} Acm^{-2} and 7.01×10^{-5} Acm^{-2}, respectively. The fill factor (*FF*) value can be calculated by using J_m, V_m, J_{sc}, and V_{oc} values ($FF = (V_m \times J_m)/(V_{oc} \times J_{sc})$) [35]. The *FF* values of S3 and S4 diodes were calculated as 0.20 and 0.24, respectively.

4 Conclusion

The structural, morphological, and optical properties of un-doped and Yb (1, 2, 3, 4, and 5 wt%)-doped CuO thin films were investigated. These thin films were deposited on the glass substrate by the USP method. The peaks belonging to the (−111) and (111) planes were observed from the XRD patterns of the films. According to AFM analysis, the surfaces of the produced CuO thin films were not smooth and the roughness increased as the Yb doping ratio increased. From the SEM images, it was found that the surface of 3 wt% Yb doped CuO thin films is more homogeneous coated than the other films, and the surfaces of 4 wt% and 5 wt% Yb doped CuO thin films have a porous structure. The average transmittance values in the visible (390–780 nm) region were calculated for all thin films. E_g values of thin films were calculated by using the Tauc plot. Therefore, the *p-n* junction diodes were produced by depositing 3 wt% Yb-doped CuO thin films on non-etched and KOH-etched *n*-Si wafers by the USP method. The changes in the electrical parameters of these diodes under illumination were investigated. The S3 and S4 diodes exhibited photovoltaic behavior. These diodes show promise for photodiode applications in the opto-electronics industry.

Author contributions

HEL: studies conceptualization, writing (original draft) the manuscript, the experimental process, and the data collection and analysis.

Funding

Data availability

The data that support the findings of this study are available from the corresponding author, upon reasonable request.

Declarations

Conflict of interest The author declares that I have no known competing financial interests or personal relationships that could have appeared to influence the work reported in this paper.

References

1. C.T. Sah, Characteristics of the metal-oxide-semiconductor transistors. IEEE Trans. Electron. Devices **11**, 324–345 (1964)
2. D. Naveena, T. Logu, R. Dhanabal, K. Sethuraman, A.C. Bose, Comparative study of effective photoabsorber CuO thin films prepared via different precursors using chemical spray pyrolysis for solar cell application. J. Mater. Sci. : Mater. Electron. **30**, 561–572 (2019)
3. N.R. Elezovic, V.R. Radmilovic, N.V. Krstajic, Platinum nanocatalysts on metal oxide based supports for low temperature fuel cell applications. RSV Adv. **6**, 6788–6801 (2016)
4. S. Demirezen, A. Eroğlu, Y. Azizian-Kalandaragh, Ş Altındal, Electric and dielectric parameters in Au/n-Si (MS) capacitors with metal oxide-polymer interlayer as function of frequency and voltage. J. Mater. Sci. : Mater. Electron. **31**, 15589–15598 (2020)
5. J. Zhang, Z. Qin, D. Zeng, C. Xie, Metal-oxide-semiconductor based gas sensors: screening, preparation, and integration. Phys. Chem. Chem. Phys. **19**, 6313–6329 (2017)
6. Q. Zhang, K. Zhang, D. Xu, G. Yang, H. Huang, F. Nie, C. Liu, S. Yang, CuO nanostructures: synthesis, characterization, growth mechanisms, fundamental properties, and applications. Prog Mater. Sci. **60**, 208–337 (2014)
7. A.M. Ahmed, E.M. Abdalla, M. Shaban, Simple and low-cost synthesis of Ba-doped CuO thin films for highly efficient solar generation of hydrogen. J. Phys. Chem. C **124**, 22347–22356 (2020)
8. M.R. Waikar, A.A. Shaikh, R.G. Sonkawade, The supercapacitive performance of woollen-like structure of CuO thin films prepared by the chemical method. Vacuum **161**, 168–175 (2019)
9. S. Baturay, A. Tombak, D. Kaya, Y.S. Ocak, M. Tokus, M. Aydemir, T. Kilicoglu, Modification of electrical and optical properties of CuO thin films by Ni doping. J. Sol-Gel Sci. Technol. **78**, 422–429 (2016)
10. K. Santra, C.K. Sarkar, M.K. Mukherjee, B. Ghosh, Copper oxide thin films grown by plasma evaporation method. Thin Solid Films **213**, 226–229 (1992)
11. D. Naveena, T. Logu, K. Sethuraman, A.C. Bose, Significant enhancement of photo-physicochemical properties of Yb doped copper oxide thin films for efficient solid-state solar cell. J. Alloys Compd. **795**, 187–196 (2019)
12. I. Singh, G. Kaur, R.K. Bedi, CTAB assisted growth and characterization of nanocrystalline CuO films by ultrasonic spray pyrolysis technique. Appl. Surf. Sci. **257**, 9546–9554 (2011)
13. S.C. Tsai, Y.L. Song, C.S. Tsai, C.C. Yang, W.Y. Chiu, H.M. Lin, Ultrasonic spray pyrolysis for nanoparticles synthesis. J. Mater. Sci. **39**, 3647–3657 (2004)
14. D. Bayuwati, Comparison of SnO2/Si-n thin films deposited by pneumatic spray pyrolysis technique with that deposited by ultrasonic spray pyrolysis technique. Indones J. Mater. Chem. **43**, 241–245 (2008)
15. M.L. Zeggar, L. Chabane, M.S. Aida, N. Attaf, N.Zebbar, solution flow rate influence on properties of copper oxide thin films deposited by ultrasonic spray pyrolysis. Mater. Sci. Semicond. Process. **30**, 645–650 (2015)
16. H.Z. Asl, S.M. Rozati, Spray deposited nanostructured CuO thin films: influence of substrate temperature and annealing process. Mater. Res. **21**, e20170754 (2018)
17. P. Venkateswari, P. Thirunavukkarasu, M. Ramamurthy, M. Balaji, J. Chandrasekaran, Optimization and characterization of CuO thin films for p-n junction diode application by JNSP technique. Optik **140**, 476–484 (2017)
18. D.P. Dubal, G.S. Gund, C.D. Lokhande, R. Holze, CuO cauliflowers for supercapacitor application: novel potentio-dynamic deposition. Mater. Res. Bull. **48**, 923–928 (2013)
19. W. Yin, J. Yang, K. Zhao, A. Cui, J. Zhou, W. Tian, W. Li, Z. Hu, J. Chu, High responsivity and external quantum efficiency photodetectors based on solution-processed Ni-doped CuO films. ACS Appl. Mater. Interfaces **12**, 11797–11805 (2020)
20. R.D. Shannon, Revised effective ionic radii and systematic studies of interatomic distances in halides and chalcogenides. Acta Cryst. **32**, 751–767 (1976)
21. D.A. Aldemir, Structural, morphological and optical properties of Yb2Cu2O5 thin films. J. Mater. Sci. **30**, 19457–19462 (2019)
22. Y. Zhang, Electronegativities of elements in valence states and their applications. 1. Electronegativities of elements in valence states. Inorg. Chem. **21**, 3886–3889 (1982)

23. H. Angermann, W. Henrion, M. Rebien, A. Röseler, Wet-chemical preparation and spectroscopic characterization of Si interfaces. Appl. Surf. Sci. **235**, 322–339 (2004)

24. J. Naktiyok, A.K. Özer, Synthesis of copper oxide (CuO) from thermal decomposition of copper acetate monohydrate $(cu(CH_3COO)_2.H_2O)$. OHU J. Eng. Sci. **8**, 1292–1298 (2019)

25. V. Saravan, P. Shankar, G.K. Mani, J.B.B. Rayappan, Growth and characterization of spray pyrolysis deposited copper oxide thin films: influence of substrate and annealing temperatures. J. Anal. Appl. Pyrolysis **111**, 272–277 (2015)

26. B.D. Cullity, *Elements of X-ray Diffraction* (Addison-Wesley Publishing, Boston, 1956)

27. L. Debbichi, M.C. Marco de Lucas, J.F. Pierson, P. Krüger, Vibrational properties of CuO and Cu_4O_3 from first-principles calculations, and Raman and infrared spectroscopy. J. Phys. Chem. C **116**, 10232–10237 (2012)

28. K. Ungeheuer, K.W. Marszalek, M. Mitura-Nowak, M. Perzanowski, P. Jelen, M. Marszalek, M. Sitarz, Influence of Cr ion implantation on physical properties of CuO thin films. Int. J. Mol. Sci. **23**, 4541 (2022)

29. Z. Shaghaghi, A.R. Amani-Ghadim, M. Seraji, Structural properties and photocatalytic degradation efficiency of CuO and erbium doped CuO nanostructures prepared by thermal decomposition of some Cu-salophen type complexes as precursors. Mater. Chem. Phys. **243**, 122635 (2020)

30. J. Tauc, R. Grigorovici, A. Vancu, Optical properties and electronic structure of amorphous germanium. Phys. Status Solidi B **15**, 627–637 (1966)

31. M.K. Basher, M.K. Hossain, M.J. Uddin, M.A.R. Akand, K.M. Shorowordi, Effect of pyramidal texturization on the optical surface reflectance of monocrystalline photovoltaic silicon wafers. Optik **172**, 801–811 (2018)

32. E.H. Rhoderick, R.H. Williams, *Metal-semiconductor contacts*, 2nd edn. (Clarendon, Oxford, 1988)

33. D.K. Schroder, *Semiconductor material and device characterization*, 3rd edn. (Wiley, New Jersey, 2006)

34. H.E. Lapa, A. Kökce, D.A. Aldemir, A.F. Özdemir, The response of high barrier Schottky diodes to light illumination. J. Mater. Sci. **32**, 4448–4456 (2021)

35. J. Allison, *Electronic engineering semiconductors and devices*, 2nd edn. (McGraw-Hill, London, 1990)